Available at www.sciencedirect.com

ScienceDirect

journal homepage: www.elsevier.com/locate/watres

Coagulation dynamics of fractal flocs induced by enmeshment and electrostatic patch mechanisms

Jr-Lin Lin[a], *Chihpin Huang*[a,*], *Ching-Ju M. Chin*[b], *Jill R. Pan*[c]

[a]*Institute of Environmental Engineering, National Chiao-Tung University, 75 Po-Ai Street, Hsinchu 300, Taiwan*
[b]*Institute of Environmental Engineering, National Central University, Jungli, Taiwan*
[c]*Department of Biological Science and Technology, National Chiao-Tung University, Hsinchu, Taiwan*

ARTICLE INFO

Article history:
Received 5 February 2008
Received in revised form
7 July 2008
Accepted 31 July 2008
Published online 23 August 2008

Keywords:
PACl
Coagulation
Kaolin aggregates
Fractal dimension
Wet SEM

ABSTRACT

The size and structure of flocs during floc formation were monitored for various coagulation mechanisms. Two distinctive mechanisms, namely, enmeshment and electrostatic patch, govern the dynamics of kaolin particles coagulation by polyaluminum chloride (PACl). They were investigated by small angle static light scattering (SASLS) and solid-state ^{27}Al NMR. In addition, a novel wet SEM (WSEM) was used in-situ to image the morphology of the aggregate in aqueous solution. Synthetic suspended particles were coagulated by two PACl products, a commercial product (PACl) and one laboratory product (PACl-E). The PACl-E contained more than 60% Al_{13} while the PACl contained only 7% Al_{13}, with large percentage of colloidal Al. For coagulation by PACl at neutral pH and high dosage where the strong repulsion between particles occurs, the enmeshment ruled by reaction-limited aggregation (RLA) results in larger sweep flocs as well as higher fractal dimensional structure. For coagulation by PACl-E at alkaline pH and low dosage, the flocs were coagulated predominately by electrostatic patch with Al_{13} aggregates. At such condition, it is likely that diffusion-limited aggregation (DLA) predominately rule PACl-E coagulation. The fractal dimension (D_s) values of PACl and PACl-E flocs formed at enmeshment and electrostatic patch increased with dosage, respectively. When breakage of flocs occurs, the breakage rate of PACl-E flocs is slower than that of sweep flocs. By WSEM imaging, the adsorption of spherical Al precipitates onto the particles was observed to form sweep flocs with a rough and ragged contour, while the PACl-E flocs were formed with a smooth and glossy structure.

1. Introduction

Coagulation is the most important process to remove the colloidal particles in conventional water treatment plants. In the past decades, inorganic polymer flocculants such as prehydrolyzed polyaluminum chloride (PACl) has been widely adopted in water treatment. Effective coagulation by PACl depends on the interaction between hydrolyzed aluminum and particles in raw water. Many studies have proven that Al(III) species is driven into various hydrolyzed Al species such as $Al(OH)^{+}$, $Al(OH)^{2+}$, $Al_2(OH)_2^{4+}$, $Al_3(OH)_4^{5+}$, $Al_{13}O_4(OH)_{24}(H_2O)_{12}^{7+}$ (Al_{13}), and aluminum hydroxide ($Al(OH)_3$) in the hydrolysis processes, which are governed by the [OH^-/Al] ratio (Akitt and Farthing, 1981; Bertsch et al., 1986; Bottero et al., 1987). The polymeric portion in PACl, which is prehydrolyzed by controlling adequate [OH^-/Al] ratio in hydrolysis

* *Corresponding author*. Tel.: +886 3 5726463; fax: +886 3 5725958.
E-mail address: cphuang@mail.nctu.edu.tw (C. Huang).
0043-1354/$ – see front matter © 2008 Elsevier Ltd. All rights reserved.
doi:10.1016/j.watres.2008.07.043

processes, is responsible for the removal of particles via charge neutralization (Lin et al., 2008; Wang and Hsu, 1994).

The interactions of the hydrolyzed Al species with particles during coagulation in the water are contributed by different coagulation mechanisms, which thereafter affect the aggregation kinetics of particles and the structure of aggregates (Van Benschoten and Edzwald, 1990; Licskó, 1997). The destabilization of suspended particles in coagulation is generally elucidated in terms of two distinct mechanisms, charge neutralization and sweep flocculation (enmeshment) (Duan and Gregory, 2003). Dentel (1988) has also proposed that the precipitation charge neutralization which suggests coagulation by charge neutralization can be explained as partial coverage of negatively charged particle surface by positively charged aluminum hydroxide. In addition, electrostatic patch caused by aluminum hydroxide precipitate has been proposed for the PACl coagulation in the presence of anion (Wang et al., 2002). However, the aggregation kinetics is highly related to the coagulation mechanisms, which significantly affect the size and the structure of aggregates (Berka and Rice, 2005; Yu et al., 2006).

So far, research has demonstrated that charge neutralization induced by PACl can bring about more rapid particle aggregation than enmeshment induced by alum (Matsui et al., 1998), and the aggregates induced by charge neutralization become more compact that resist shear stress (McCurdy et al., 2004). PACl coagulants from different sources contain various portions of monomeric and polymeric Al species that will affect the coagulation mechanism such as enmeshment, precipitation charge neutralization and electrostatic patch. Those mechanisms substantially influence the aggregation kinetics that is dependent of the Al speciation of PACls, operational pH and PACl dosage (Ye et al., 2007). Although the structure, strength and growth kinetics of alum–kaolin flocs have been well investigated (Francois, 1987, 1988; Chakraborti et al., 2003), limited studies have paid attention to the relationship between aggregation kinetics and the structure of flocs in PACl coagulation induced by enmeshment and electrostatic patch.

Flocs formed by coagulation in water and wastewater treatment are considered to be the fractal structure (Thomas et al., 1999). The observation of the floc structure is essential to realize the coagulation kinetics. There are some studies that investigated the size and structure of aggregates formed in coagulation of colloids by optical microscope (OM), scanning electron microscope (SEM), transmission electron microscope (TEM), and atomic force microscope (AFM) (Cornelissen et al., 1997; Ferretti et al., 2003; Zbik and Horn, 2003). Other studies also used a non-intrusive image analysis technique to observe and analyze the structure of wet aggregates in coagulation process (Chakraborti et al., 2000; Chakraborti et al., 2007). However, in-situ high-resolution image of wet aggregates has not been obtained yet. Recently, the wet SEM (WSEM), a novel technology that allows direct imaging of fully wet samples such as cement and clay in a conventional SEM (Katz et al., 2007; Li et al., 2007), which, however, has not been applied on the in-situ observation of the aggregates coagulated by PACl containing various Al species.

In this study, the relationship between the dynamics of aggregation and the structure of aggregates formed by PACl coagulation by enmeshment and electrostatic patch was investigated via the in-situ diagnostic technology. A commercial PACl with high contents of monomeric and aluminum hydroxide species and one laboratory product (term as PACl-E) with high portion of polymeric species were applied in a kaolin suspension. The solid-state ^{27}Al NMR was employed to identify the Al speciation of flocs coagulated with PACl and PACl-E. The in-situ monitors for flocs growth by PACl and PACl-E coagulation at various dosages were carried out by small angle static light scattering (SASLS). Moreover, the wet SEM (WSEM) was used to directly observe wet flocs formed at the end.

2. Material and methods

2.1. Kaolin suspension

The purified kaolin (Sigma Chemical Co., USA) was mixed with RO water and dispersed for 30 min to a concentration of 2.5 g/L. After 24 h settling, the supernatant was used as the synthetic stock solution, from which the RO water was added to prepare the turbid water samples to the desired turbidity of 50 NTU, which is about 20.3 mg/L. Particle size distribution of the synthetic suspension was analyzed by a particle size analyzer (Master 2000, Malvern Inc., UK) and a laser zeta analyzer (Zetasizer nano ZS, Malvern Inc., UK). The mean particle size of the synthetic water sample was 2.9 μm. The specific conductivity of the working suspension was adjusted by 10^{-3} M $NaClO_4$ solution (Merck, Inc., USA) and the alkalinity was adjusted by adding 10^{-3} M Na_2CO_3 (Merck, Inc., USA).

2.2. Characterization of coagulants

Two PACls were used in this study. The reagent-grade PACl ($Al_2O_3 = 10\%$) was purchased from Showa Chemicals Inc., which was designated as PACl in this article. Another PACl named PACl-E, made by an electrochemical process, was obtained as a gift from the Research Center for Eco-environmental Sciences, Chinese Academy of Sciences in China. The [OH^-/Al] ratios of PACl and PACl-E are 1.4 and 2.1, respectively. The working solutions containing 1000 mg/L Al were freshly prepared from the stock solution before each test. Aluminum concentration was analyzed by an inductive coupled plasma atomic emission spectrometry (ICPAES) (JY24, Jobin-Yvon Inc., France). The Al speciation of PACl and PACl-E was identified by both Ferron assay and ^{27}Al nuclear magnetic resonance (NMR) method.

In this study, simplified Ferron assay was used to quantify aluminum species (Wang et al., 2004). The aluminum species was quantified by the timed absorbance at 366 nm with a UV–visible spectrometer (U3010, Hitachi Inc., Japan). Based on the kinetics of the reactions between the aluminum species and Ferron agent, the hydrolyzed Al species can be categorized into three groups, monomeric (Al_a), polycations (Al_b), and colloidal (Al_c). The absorbances in the first 1 min and from 1 min to 2 h were assigned to Al_a and Al_b, respectively. And Al_c was obtained by subtracting Al_a and Al_b from the total Al. The total aluminum concentration of the solution was maintained at 3.7×10^{-4} M for the Ferron test.

The distributions of hydrolyzed species of PACl and PACl-E in solution were also determined with a 500 MHz ^{27}Al NMR (Uniytinova-500, Varian, USA). The operation parameters for the NMR analysis are spectrometer frequency, solvent, and temperature, which are 130.246 MHz, D_2O, and 298 K. A 5-mm sample tube (Wilmad 507-pp, SP Industries Inc., USA) containing 3 mL Al solution and a 4.2-mm sample tube (Wilmad WGS-5BL, SP Industries Inc., USA) containing 1 mL of 0.05 M $Al(OD)_4^-$ solution were inserted together as the inner standard. The chemical shift of $Al(OD)_4^-$ is at 80 ppm. The signals in the proximity of 0, 3–4, and 62.5 ppm represent monomeric Al (Al_m), dimeric Al (Al_2), and tridecamer Al_{13}, respectively. The concentration of each species was determined by the ratio of the integrated intensity of the corresponding peak to that of $Al(OD)_4^-$ at 80 ppm. The amount of the undetectable species (denoted as Al_u) is obtained by subtracting the sum of the detected Al species from the total Al concentration.

The results of Al speciation for both coagulants are summarized in Table 1. By Ferron assay, the major Al species of PACl are the monomeric Al (Al_m) and Al_c ($Al(OH)_3$) while the majority of Al species in PACl-E is found to be Al_b. The distributions of Al_m and Al_{13} measured by ^{27}Al NMR correspond to the distributions of Al_a and Al_b obtained by Ferron assay, respectively. Although there is a little discrepancy between the composition of Al_b and Al_{13}, both methods confirm that PACl-E contains high contents of Al_{13} exceeding 60% of total Al concentration. Other studies have also indicated that Al_{13} can be roughly represented by Al_b (Liu et al., 1999; Parker and Bertsch, 1992; Shi et al., 2007).

2.3. Coagulation experiment

Standard jar test was conducted in a 1-L beaker to evaluate the coagulation efficiency. An initial rapid mixing was conducted at 200 rpm ($G = 350\ s^{-1}$) for 1 min followed by a slow mixing at 30 rpm ($G = 25\ s^{-1}$) for 20 min. The zeta potential was measured immediately without dilution after the rapid mixing. The suspension was left undisturbed for 20 min. After settling, the residual turbidity (RT) of the supernatant was measured. All experiments were conducted at room temperature and all coagulant dosages used in this study were in the unit of mg/L as Al.

2.4. Measurement of aggregates' size and structure

A particle size analyzer (Mastersizer 2000, Malvern, UK) with a small angle static light scattering (SASLS) was used to directly monitor the dynamics of aggregate growth during coagulation process and the structure of kaolin particle aggregates. The similar jar tests were performed to observe the kinetics of coagulation for the study. During coagulation, the suspension was pumped to the SASLS by a peristaltic pump (EW-7553-70, Cole-Parmer Instrument Co., USA) with a Tygon tubing (Masterflex-06409-16, Cole-Parmer Instrument Co., USA) of I.D. 3.1 mm, and the sample was recycled back to the mixing vessel at a flow rate of 20 mL/min. The shear and disruption of aggregates in such setup are negligible.

The SASLS has been extensively employed to evaluate the size of particles and aggregates in various suspensions, such as kaolin, latex, and aluminum suspension (Waite et al., 2001; Berka and Rice, 2005). The scattered light intensity I is measured as a function of the magnitude of the scattering wave vector, Q. The relationship between the scattered intensity from the aggregate, $I(Q)$, and the Q is given by (Lin et al., 1989)

$$I(Q) \propto Q^{-D_f} \tag{1}$$

where

$$Q = \frac{4\pi n \sin(\theta/2)}{\lambda} \tag{2}$$

Here, n is the refractive index of the fluid, λ is the wavelength in vacuum of the laser light used, and θ is the scattering angle. This relationship is valid when the length scale of 1/Q is much larger than the primary particles and much smaller than aggregates. The mass fractal dimension D_f can be estimated from the absolute slope of log $I(Q)$ versus log Q by fitting a straight line through the fractal region of scattering plot. Although the diameter of the primary particles used in this study is larger than the lasers wavelength, the scattering exponents, SE, obtained from SASLS (i.e. D_s) do relate to the structure properties of primary flocs rather than to that of the entire flocs, which can be explained by the existence of two-level floc structural model that is derived by other investigators (Wu et al., 2002). In this study, the SASLS experiments have been restricted to the 10^{-3}–$4.5 \times 10^{-4}\ nm^{-1}$ Q range to allow the power law regime for the structural analysis of primary flocs. Many studies also have successfully used SASLS to evaluate the fractal dimensions of the floc aggregated from micro-scale primary particles in coagulation process (Annadurai et al., 2004; Chu et al., 2004; Yu et al., 2006). Therefore, the values of D_s measured here are comparable.

2.5. Solid-state ^{27}Al magic-angle spinning nuclear magnetic resonance

The solid-state magic-angle spinning nuclear magnetic resonance (MAS-NMR) spectra were recorded by a Bruker

Table 1 – Characteristics of coagulants by Ferron assay and ^{27}Al NMR method

Coagulants	γ[a]	pH	Ferron assay (Al, %)			^{27}Al NMR (Al, %)		
			Al_a	Al_b	Al_c	Al_m	Al_{13}	Al_u
PACl	1.4	3.80	42.3	8	49.7	38.4	6.8	54.8
PACl-E	2.1	4.06	19	65.8	15.2	16.6	60	23.4

a γ: $[OH^-/Al]$.

instrument (DSX-400WB, Bruker, Germany) in 4 mm rotors, and the ^{27}Al spectra were recorded at 104.1 MHz. The solid-state ^{27}Al MAS-MNR was performed on freeze-dried PACl and PACl-E floc samples at various PACl and PACl-E dosages. The PACl and PACl-E flocs formed after coagulation were separated immediately by freeze-drying over 24 h with a vacuum refrigerating instrument (FD2-D, Kingmech Co., Ltd, Taiwan).

2.6. *Wet scanning electron microscope (WSEM)*

Flocs formed after PACl and PACl-E coagulation were readily withdrawn into a sealed specimen capsule (QX-102, Quantomix Co. Ltd, Israel) and were protected from vacuum in the microscope by an electron-transparent partition membrane. The detail descriptions of the specimen capsule were presented elsewhere (Katz et al., 2007). After the placement of samples, the morphology of the wet aggregates was observed by a conventional scanning electron microscope (SEM) (5136LS, Tescan, Czech).

3. Results and discussion

3.1. *pH effects on the coagulation efficiency*

The changes in zeta potential (ZP) and residual turbidity (RT) during PACl and PACl-E coagulation are presented in Fig. 1. The dosage of coagulant is controlled at 1 mg/L here. There are marked discrepancies on pH regions of efficient coagulation between PACl and PACl-E. For PACl coagulation, the efficient pH region ranges from 7 to 10. The pH for the optimum turbidity removal coincides with the pH at which the ZP closes to zero. The efficient turbidity removal also occurs at pH 7.5 and pH 9, where the ZP of suspended particles is around 10 mV and −20 mV, respectively. Al(III) species can transform into voluminous amorphous aluminum hydroxide ($Al(OH)_{3(am)}$) at neutral pH (Van Benschoten and Edzwald, 1990). For the PACl applied here, the major species are Al_c (colloidal Al) with more than 50% of total Al concentration and Al_a (monomeric Al) that can further hydrolyze and form $Al(OH)_{3(am)}$ at neutral pH, as reported in previous study (Lin et al., 2008). Thus, PACl coagulation at neutral pH favors enmeshment even though the charge reversal occurs. At alkaline pH, the particles can be destabilized by electrostatic patch of $Al(OH)_3$ due to adsorption of precipitate, and then the growth of flocs is formed through precipitation charge neutralization (Dentel, 1988). Therefore, the particles are destabilized effectively at alkaline pH even though the ZP of particles is negative. However, the positive charge of aluminum hydroxide precipitate becomes gradually neutralized with increasing pH, and then the influence of electrostatic patch lessens, which results in the increase of residual turbidity with pH.

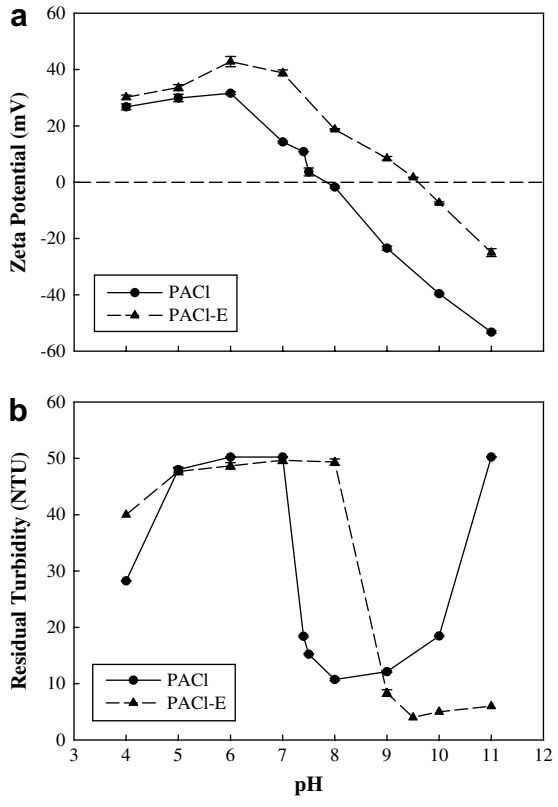

Fig. 1 – pH effects on the residual turbidity and the zeta potential for PACl and PACl-E coagulation at the dosage of 1 mg/L as Al: (a) zeta potential (b) residual turbidity.

For PACl-E coagulation, the optimum turbidity removal has been obtained when the pH is higher than 9 in which the ZP closes to zero. Because the PACl-E contains Al_{13} with more than 60% of total Al concentration, indicating the PACl-E has strong charge neutralization ability, the particles can be rapidly restabilized at low pH, while still keep coagulation efficient at high pH. The coagulation efficiency of PACl-E is superior to that of PACl which also occurs when pH is higher than 10 where the ZP is rather negative, which implies the more particles are destabilized predominately by electrostatic patch. Since Al_{13} favors aggregation when pH is over 6 (Furrer et al., 1992), Al_{13} aggregates are thus easily formed at alkaline pH at which the Al_{13} molecules are mainly absorbed onto the isolated regions of particles with negative surface charge and then further restructure and aggregate to form Al_{13} aggregates (Ye et al., 2007; Lin et al., 2008). At such condition, some regional charge heterogeneity can occur, which results in electrostatic patch (Gregory, 1973) As a result, PACl-E coagulation could be favorable for particle destabilization at alkaline pH to form larger flocs by electrostatic patch with larger Al_{13} aggregates, resulting in more efficient turbidity removal. The results show that either charge neutralization or electrostatic patch is the major coagulation mechanisms for PACl-E coagulation at alkaline pH.

3.2. *Particle destabilization*

The dosage of coagulant also influences the amount of hydrolyzed Al species adsorbed onto the surface of particles and the conformation of hydrolyzed polymeric Al species adhered to the surface of particles; as a consequence, the mechanism of coagulation by polymeric species is affected (Zhou and Franks, 2006). To understand the dosage effects on the particle destabilization at either enmeshment or electrostatic patch with Al_{13} aggregates, the coagulation performances of PACl and PACl-E are evaluated at pH 7.5 and pH 10, respectively. The changes in the RT and ZP with dosage for

PACl and PACl-E coagulation are illustrated in Fig. 2. For coagulation by PACl, as shown in Fig. 2(a), the removal of turbidity increases with dosage, which accompanies the increasing ZP. The efficient turbidity removal still occurred at high dosage, even though the charge reversal of particles takes place, which is attributed to the occurrence of enmeshment.

By contrast, the turbidity decreases rapidly after the addition of PACl-E at pH 10, and then reaches a minimum. The magnitude of the negative ZP slightly decreases with dosage at low dosage (<2 mg/L), while the negative ZP nearly levels off with changes in the dosage at high PACl-E dosage, as seen as Fig. 2(b). The plateau of almost zero ZP at high PACl-E dosage implies that the charge neutralization ability of Al_{13} is reduced, which is ascribed to the further hydrolysis of Al_{13} or rearrangement of Al_{13} subunits (Bottero et al., 1987; Bertsch, 1987). Al_{13}, which has a +7 valence, can be deprotonated to release the protons in pairs and yield the weakly positively charged Al_{13} while the pH and Al_{13} concentration are raised (Furrer et al., 1992). However, previous study has shown that Al_{13} aggregates still have certain charge neutralization ability to aggregate particles (Chen et al., 2006). Thus, the Al_{13} aggregates with less surface positive charge is easily formed at alkaline pH for PACl-E coagulation and cannot cause the strong charge neutralization, which leads to nearly zero ZP of the particles, even though the dosage is continuously increased.

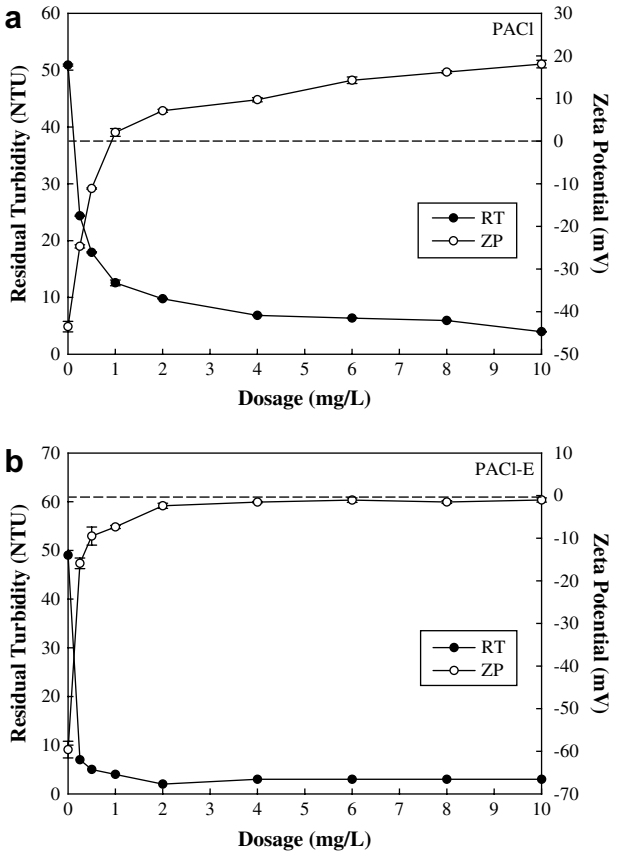

Fig. 2 – Dosage effects on the residual turbidity and zeta potential for (a) PACl coagulation at pH 7.5 and (b) PACl-E coagulation at pH 10.

To further verify the predominant mechanism in PACl and PACl-E coagulation, the solid-state ^{27}Al NMR was used to identify the Al speciation within the aggregates. Fig. 3 shows the ^{27}Al NMR spectra obtained for PACl coagulation at neutral pH and PACl-E coagulation at alkaline pH at different Al concentrations. An intensive peak at 0 ppm is found within PACl aggregates, while a weak peak at 33 ppm is only observed when the dosage is increased. On the other hand, the spectra for PACl-E aggregates formed at 8 mg/L exhibit two distinct resonances at about 0 ppm and 63 ppm, whereas the spectra for PACl-E aggregates formed at 1 mg/L of dosage displayed one prominent resonance at 0 ppm and very weak resonance at 63 ppm.

The symmetric peak at 0 ppm corresponds to octahedrally coordinated aluminum and the peak at 63 ppm corresponds to tetrahedral aluminum (Bottero et al., 1980). The 33 ppm signal of PACl aggregates, indicating a five-coordinate Al, is attributed to the process of freeze-drying of sediments (Wood et al., 1990). Only the octahedral aluminum is found in PACl aggregates even at high dosage, which suggests enmeshment plays an important role during PACl coagulation at neutral pH. For PACl-E coagulation, because of the weaker surface charge of the Al_{13} at alkaline pH, less Al_{13} could react with the negatively charged kaolin particles, which leads to the unobvious 63 ppm signal. However, the unambiguous resonance at 63 ppm is detected when the dosage of coagulant increases. Since the central AlO_4 is almost unreactive when the aggregation of Al_{13} occurs (Phillips et al., 2000), the 63 ppm signal remains intensive even though the aggregated Al_{13} is formed. The results show that the flocs formation by PACl coagulation at neutral pH relies on enmeshment with $Al(OH)_3$ regardless of the dosage applied, while electrostatic patch with Al_{13} aggregates in PACl-E coagulation at alkaline pH is responsible for particle aggregation.

3.3. *Coagulation kinetics*

Coagulation mechanisms could significantly affect the coagulation kinetics and dominate the flocs' size and structure.

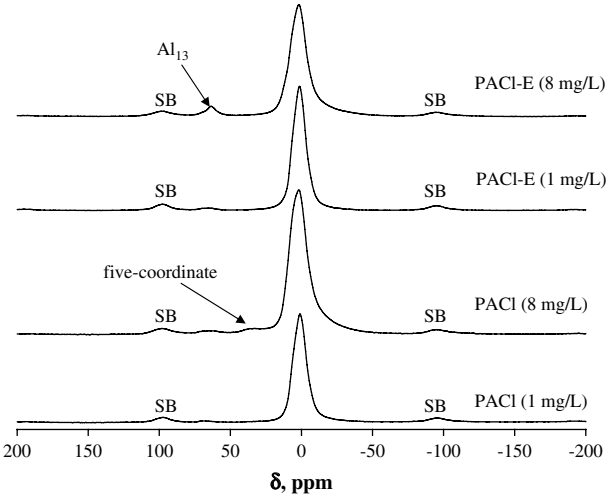

Fig. 3 – Solid-state ^{27}Al MAS-NMR spectra of freeze-dried kaolin flocs coagulated by PACl and PACl-E at various dosages.

Fig. 4 shows the growth profile of the flocs for PACl coagulation at neutral pH and PACl-E coagulation at alkaline pH, where the flocs' size is presented by the median equivalent diameter (d_{50}). There marked differences between the growth trends of PACl flocs (sweep flocs) and PACl-E flocs. For PACl coagulation, the growth rate of the flocs raises with dosage. Moreover, more particles are destabilized throughout efficient collisions when the dosage is increased, which leads to abrupt increase of the aggregation rate at the initial aggregation. The most dramatic observation is that, at high dosage (8 mg/L) the flocs' size sharply increases at the initial aggregation and then reaches a maximum, but decreases gradually over time, which could be explained by the breakage of flocs during flocculation.

It has been accepted that the growth of flocs depends on a balance between the formation and breakage of flocs (Biggs and Lant, 2000; Ducoste and Clark, 1998). During the rapid initial formation of sweep flocs, the flocculation of primary flocs dominates the evolution of particles size, then the influence of breakage increases as flocs' size increases until a steady-state size is approached. As the largest flocs induced by strong enmeshment at high dosage are formed, the number of the primary particles will decrease to a minimum before the steady-state flocs are reached, which results in the significant decrease of collision rate as well as the increase in breakage rate. Meanwhile, the more dosage is applied for PACl coagulation, the larger the sweep flocs that contain large porosity and then are easily broken by surface erosion of eddies splitting (i.e. large-scale fragment) that is dependent of flocs' structure (Jarvis et al., 2005). Consequently, the breakage rate of the sweep flocs at high PACl dosage is faster. Because the breakage of flocs is relatively heavy at high dosage where the d_{50} size of flocs decreases from 450 μm to 350 μm, the possible breakage mode is surface erosion resulting in an increase in the small particle size ranges.

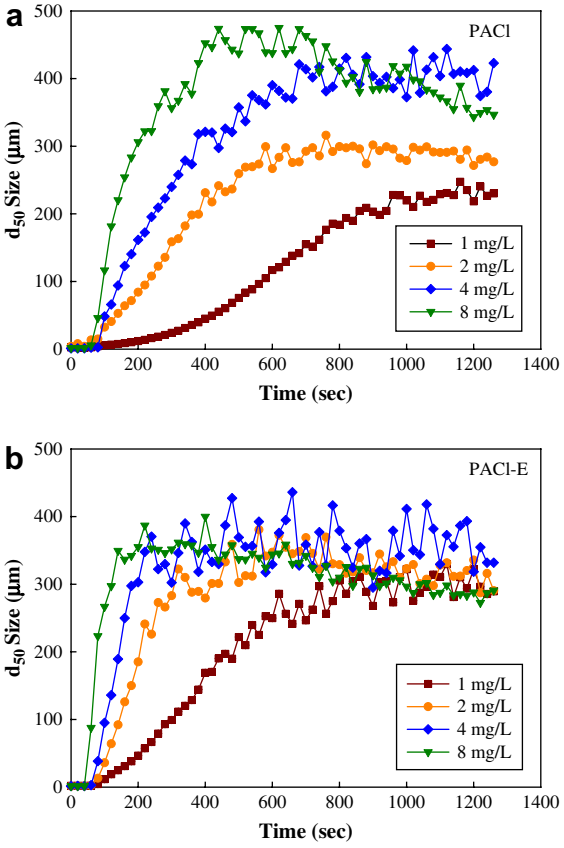

Fig. 4 – The aggregation kinetics of kaolin particles induced by (a) PACl coagulation at pH 7.5 and (b) PACl-E coagulation at pH 10.

For PACl-E coagulation, the size of flocs also increases with dosage, and the equilibrium d_{50} size of flocs coagulated with various dosages remains 300–400 μm. At the same low dosage (1 mg/L), the d_{50} size of flocs coagulated by PACl-E is much smaller than that of PACl in response to electrostatic patch induced with Al_{13} aggregates. In addition, since PACl coagulation favors enmeshment, larger sweep flocs formed at high dosage are observed as a result of the occurrence of abundant $Al(OH)_3$. However, the initial growth of PACl-E flocs is more rapid than that of sweep flocs at various dosages studied. Enmeshment is generally slower than other coagulation mechanisms because $Al(OH)_3$ precipitates require a few seconds to form in coagulation (Letterman et al., 1973). Therefore, the PACl-E coagulation that favors charge neutralization (or electrostatic patch) can give faster particle coagulation. Meanwhile, the size of PACl-E flocs formed at 8 mg/L also decreases with slow mixing time, but the breakage rate of them is slower than that of sweep flocs. This indicates that the PACl-E flocs possess a stronger resistance to shear stress due to stronger attractive forces between particles within the PACl-E flocs under charge neutralization. Out of the minor decrease in floc size for PACl-E coagulation at high dosage, the breakage mode is inferred to be large-scale fragmentation that is the cleavage of flocs into several pieces of a size similar to parent flocs (Jarvis et al., 2005).

The results of coagulation kinetics show that the dosage of PACl strongly affects the balance between efficient collision and the breakage of the flocs. The breakage degree of flocs induced by shear stress during PACl and PACl-E coagulation is unlike due to different coagulation mechanisms. Therefore, the structure of the flocs coagulated by PACl and PACl-E will be dependent of the coagulants' dosage as well as dominant mechanisms.

3.4. *Flocs' structure*

The mean size and fractal dimension (D_s) of the flocs formed by PACl and PACl-E coagulation at various dosages are presented in Fig. 5. For PACl coagulation, the mean size and D_s of sweep flocs increase with dosage except for at the high dosage (8 mg/L) where a drop of mean size occurs (Fig. 5(a)). In theory, fractal dimensions do not change as a function of flocs' size. However, study has indicated that fractal dimension decreases as the increase of flocs' size in the coagulation of latex by using Al based coagulants (Chakraborti et al., 2000). By contrast, our results have supported the findings by Jiang and Logan (1996), which proposed that increasing flocs' size may simultaneously increase the fractal dimensions as a result of breakup and re-aggregation of larger flocs. The relationship between fractal dimensions and flocs' size could be further explained by the mode of particle aggregation. Particle

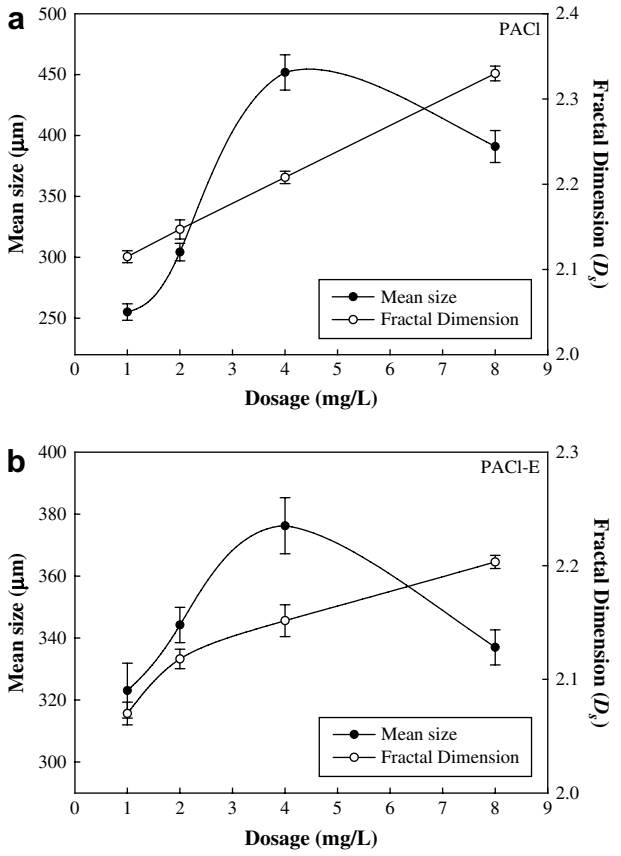

Fig. 5 – Dosage effects on the fractal dimensions (D_s) of flocs coagulated by (a) PACl at pH 7.5 and (b) PACl-E at pH 10.

aggregation is dictated by aggregation limiting regimes, including diffusion-limited aggregation (DLA), when there is no repulsive force between the colloidal particles and reaction-limited aggregation (RLA) where additional repulsive forces caused by electrostatic forces or steric interaction prevent the particles from aggregation (Elimelech et al., 1995). In addition, the variation of the fractal dimension of kaolin flocs with the change in slow mixing time can reflect the regimes of coagulation kinetics (Berka and Rice, 2005).

As shown in Figs. 2(a) and 4(a), the charge reversal of particles occurs when the dosage is higher than 1 mg/L in PACl coagulation, but the efficient aggregation and turbidity removal still occur. Because the shear stress induced by mixing overcomes the repulsion among particles during slow mixing, the particles can aggregate after encounter of each other over time, suggesting the PACl coagulation at high dosage is governed by RLA. The higher the dosage the stronger is the repulsion between particles, which causes low collision efficiency. As a result, particles or clusters need to collide many times before sticking occurs as the increase in dosage, ranging from 2 mg/L to 8 mg/L. This gives more opportunities to explore other configurations, and then particles are able to penetrate into a cluster before encountering another particle and sticking (Lin et al., 1989), as a result, more compact flocs are obtained. Furthermore, the breakage of flocs and an increase in the D_s of the sweep flocs coagulated by PACl at 8 mg/L occur with slow mixing time, as illustrated in Fig. 4(a) and Table 2, indicating the flocs are restructuring during flocs breakage process. Similar studies have been reported that a restructuring of primary particles within flocs because breakage and re-aggregation occurs in response to ambient shear (Clark and Flora, 1991; Oles, 1992). In our experiments, the rearrangement of primary particles within flocs can be caused by breakages of the flocs through a longer flocculation time and then are restructured throughout the new balance between the reformation and breakage of flocs over time. This process possibly makes flocs into a denser and more compact structure. Therefore, the D_s values of sweep flocs sharply increase from 2.2 to 2.33 when breakage occurs, as evidenced by Fig. 5(a). Contrary to high dosage, the change of the D_s values of sweep flocs formed at low dosage (1 mg/L) is not obvious with slow mixing time because restructuring caused by breakage of flocs does not occur.

Similar tendency of changes in mean size and fractal dimension of flocs is also found for PACl-E coagulation, as illustrated in Fig. 5(b). PACl-E coagulation favors electrostatic patch at low dosage or charge neutralization at high dosage. With increasing dosage, the more efficient particle coagulation is obtained due to the weaker repulsion among particles that leads to the shorter distance between particles within the flocs and thus the flocs have higher D_s. Although the PACl-E flocs experience breakage at 8 mg/L, as shown in Fig. 4(b), the almost invariant D_s of PACl-E flocs are observed to be in the range from 2.2 to 2.21 during flocs breakage. This demonstrates that an invariant structure of flocs is formed because the breakage of PACl-E flocs does not result in the occurrence of interflocs restructuring. Studies have suggested that the invariable fractal dimension of flocs represents DLA with no reconstruction and rearrangement in shear coagulation with polymers (Biggs et al., 2000; Yu et al., 2006). The change in fractal dimension of PACl-E flocs formed at low dosage is similar to that at high dosage. It is likely that the PACl-E coagulation at 8 mg/L is induced by charge neutralization at which the nearly zero charged particles can aggregate by DLA. In general, cluster–cluster flocs have fractal dimension values of around 1.8 at DLA and 2.1 at RLA, respectively (Lin et al., 1989). However, the sweep flocs and PACl-E flocs formed at RLA and DLA have higher D_s values around 2.3 and 2.2, which could be assigned to the breakage of flocs resulting particle–cluster aggregation that creates a denser internal structure within flocs.

Table 2 – Fractal dimensions (D_s) of PACl and PACl-E flocs during coagulation

Coagulants	Time (min)	Fractal dimension (D_s)[a]	
		1 mg/L	8 mg/L
PACl	10	2.09	2.28
	15	2.11	2.30
	20	2.11	2.33
PACl-E	10	2.06	2.20
	15	2.07	2.21
	20	2.08	2.21

a D_s: mean values of scattering exponent measured by SASLS.

3.5. *Morphology of flocs*

In this work, the WSEM is used to observe the morphology and main structure of primary flocs in the moist condition for the first time in order to further understand the interactions of various Al species and kaolin particles under different coagulation mechanisms induced by PACl and PACl-E. The WSEM images of sweep flocs and PACl-E flocs at low and high dosage are shown in Fig. 6. At low dosage, sweep flocs have some spherical nuclei, while contain many amorphous matters at high dosage, as shown in Fig. 6(a) and (b). Because the PACl coagulation at neutral pH undergoes enmeshment mostly, the particle can be then aggregated as sweep flocs by both surface precipitation and adsorption of amorphous hydroxide precipitate on the surface of particles (called heterocoagulation) (Chowdhury and Amy, 1991). In enmeshment, there are external particles (amorphous hydroxide precipitate), which cloud the surface where the nucleation and growth occur. Less amorphous hydroxide precipitate can only diffuse onto the particles by shear when low dosage is applied, which results in insufficient nucleation or precipitation charge neutralization induced by colloidal $Al(OH)_3$. Contrary to the low dosage, more amorphous hydroxide precipitate is formed at high dosage and covers the surface of particles, which causes the formation of larger sweep flocs with a rough and ragged contour. For PACl coagulation at 8 mg/L, when the breakage of flocs occurs, in which more floc conformations are exposed, the occurrence of particle–cluster aggregation will become relatively easier. As a result, the principal part of sweep flocs formed by PACl coagulation at such condition has a higher fractal dimensional structure.

As shown in Fig. 6(c) and (d), the flocs formed by PACl-E coagulation at 8 mg/L are larger and more compact than that at 1 mg/L. Since DLA induced by charge neutralization predominately governs the PACl-E coagulation at high 8 mg/L without structuring of flocs, where the particles attach permanently to other particles at the first contact, PACl-E flocs are possibly formed by cluster–cluster aggregation, as reported by Torres et al. (1991). However, when breakages of the flocs occur at 8 mg/L, the particle–cluster aggregation is likely formed, which results that the edge of the flocs is loosely associated but the interior is so densely packed that primary particles are not easily observed, as shown in Fig. 6(d). By contrast, the breakage of PACl-E flocs does not occur at 1 mg/L, at which the flocs formed by electrostatic patch have a more open structure in response to cluster–cluster aggregation, as indicated in Fig. 6(c). The results of WSEM imaging are in accordance with the observation from SASLS.

4. Conclusions

At neutral pH, the PACl with monomeric and colloidal Al species favors enmeshment in response to the occurrence of abundant $Al(OH)_{3(am)}$. By contrast, the PACl-E containing high percentage of Al_{13} causes either electrostatic patch or charge neutralization mechanisms with Al_{13} aggregates at alkaline pH. Electrostatic patch with Al_{13} aggregates can cause the faster coagulation than enmeshment with $Al(OH)_3$. The breakage of flocs induced by enmeshment and electrostatic patch occursat overdosing. The breakage rate of sweep flocs is faster than that of PACl-E flocs. The structures of sweep flocs

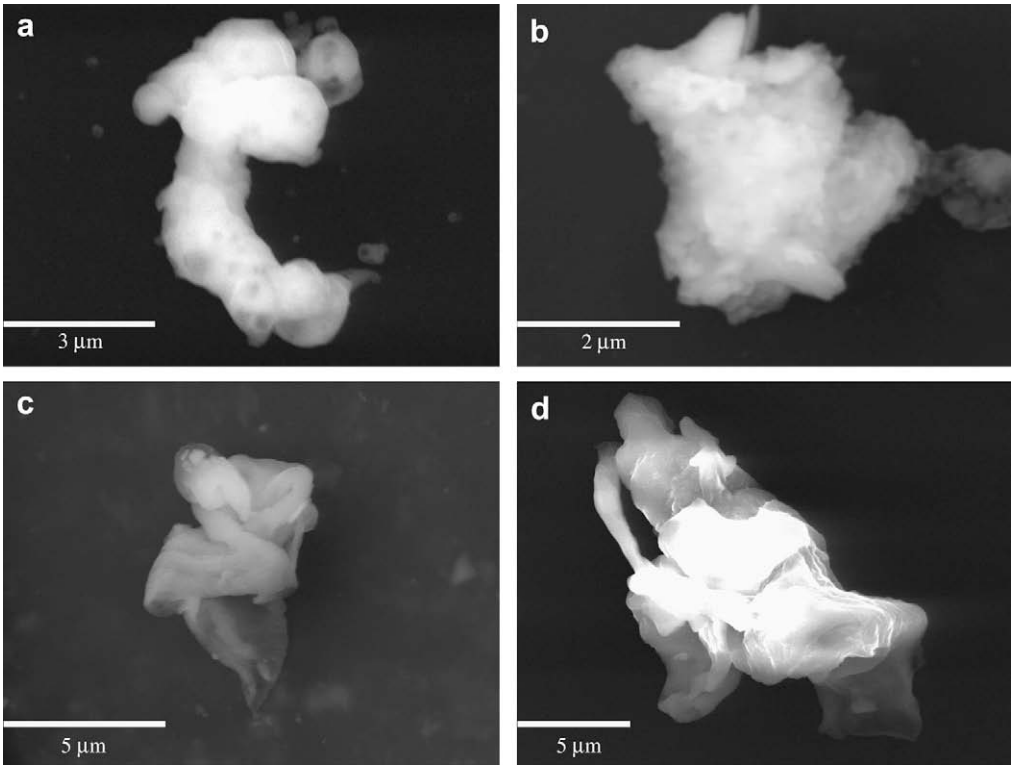

Fig. 6 – The wet SEM images of sweep flocs and PACl-E flocs formed at various dosages; PACl: (a) 1 mg/L and (b) 8 mg/L; PACl-E: (c) 1 mg/L and (d) 8 mg/L.

formed by enmeshment become denser with dosage at RLA, in which the breakage of sweep flocs can cause the increase in fractal dimension of flocs. On the other hand, PACl-E flocs formed by electrostatic patch become more compact with dosage and have a stronger resistance to shear stress during coagulation. The WSEM imaging of flocs shows that enmeshment leads to the nucleation and sweep flocs with a rough and ragged contour while electrostatic patch or charge neutralization induces flocs with a smooth and glossy surface. The results show that the aggregation modes under various destabilization mechanisms can be differentiated via the growth and structure of flocs during coagulation.

Acknowledgement

This research was supported by the grant of National Science Council, Taiwan, ROC (NSC 97-2221-E-009-069-MY3). The authors would like to extend their appreciation to Prof. Jiu-Hui Qu and Prof. Dong-Sheng Wang in RCEES-CAS (China) for providing the PACl-E powder and assisting in NMR measurements.

REFERENCES

Akitt, J.W., Farthing, A., 1981. Aluminium-27 nuclear magnetic resonance studies of the hydrolysis of aluminium (III). Part V. Slow hydrolysis using aluminum metal. J. Chem. Soc. Dalton Trans., 1624–1626.

Annadurai, G., Sung, S.S., Lee, D.J., 2004. Optimization of floc characteristics for treatment of highly turbid water. Sep. Sci. Technol. 39, 19–42.

Berka, M., Rice, J.A., 2005. Relation between aggregation kinetics and the structure of kaolinite aggregates. Langmuir 21, 1223–1229.

Bertsch, P.M., 1987. Conditions for Al13 polymer formation in partially neutralized aluminum solutions. Soil Sci. Soc. Am. J. 51 (3), 825–828.

Bertsch, P.M., Layton, W.J., Barnhisel, R.I., 1986. Speciation of hydroxyl-aluminum solutions by wet chemical and aluminum-27 NMR methods. Soil Sci. Soc. Am. J. 50 (6), 1449–1454.

Biggs, C.A., Lant, P.A., 2000. Activated sludge flocculation: on-line determination of floc size and the effect of shear. Water Res. 34, 2542–2550.

Biggs, S., Habgood, M., Jameson, G., Yan, Y.D., 2000. Aggregate structures formed via a bridging flocculation mechanism. Chem. Eng. J. 80, 13–22.

Bottero, J.Y., Axelos, M., Tchoubar, D., Cases, J.M., Fripiat, J.J., Fiessinger, F., 1987. Mechanism of formation of aluminum trihydroxide form Keggin Al_{13} polymers. J. Colloid Interface Sci. 117 (1), 47–57.

Bottero, J.Y., Cases, J.M., Fiessinger, F., Poirier, J.E., 1980. Studies of hydrolyzed aluminum chloride solutions. I. Nature of aluminum species and composition of aqueous solutions. J. Phys. Chem. 84, 2933–2939.

Chakraborti, R.K., Atkinson, J.F., Van Benschoten, J.E., 2000. Characterization of alum floc by image analysis. Environ. Sci. Technol. 34, 3969–3976.

Chakraborti, R.K., Gardner, K.H., Atkinson, J.F., Van Benschoten, J.E., 2003. Changes in fractal dimension during aggregation. Water Res. 37, 873–883.

Chakraborti, R.K., Gardner, K.H., Kaur, J., Atkinson, J.F., 2007. *In situ* analysis of flocs. J. Water Supply: Res. Technol. – AQUA 56 (1), 1–11.

Chen, Z.Y., Fan, B., Peng, X.J., Zhang, Z.G., Fan, J.H., Luan, Z.K., 2006. Evaluation of Al_{30} polynuclear species in polyaluminum solutions as coagulant for water treatment. Chemosphere 64, 912–918.

Chowdhury, Z.K., Amy, G.L., 1991. Coagulation of submicron colloids in water treatment by incorporation into aluminum hydroxide floc. Environ. Eng. Sci. 25, 1766–1773.

Chu, C.P., Lee, D.J., Peng, X.F., 2004. Structure of conditioned sludge flocs. Water Res. 38, 2125–2134.

Clark, M.M., Flora, J.R.V., 1991. Floc restructuring in varied turbulent mixing. J. Colloid Interface Sci. 147, 407–420.

Cornelissen, A., Burnett, M.G., McCall, R.D., Goddard, D.T., 1997. Structure of hydrous flocs prepared by batch and continuous flow water treatment systems and obtained by optical, electron and atomic force microscopy. Water Sci. Technol. 36 (4), 41–48.

Dentel, S.K., 1988. Application of the precipitation-charge neutralization model of coagulation. Environ. Sci. Technol. 22, 825–832.

Duan, J., Gregory, J., 2003. Coagulation by hydrolyzing metal salts. Adv. Colloid Interface Sci. 100–102, 475–502.

Ducoste, J.J., Clark, M.M., 1998. The influence of tank size and impeller geometry on turbulent flocculation: I. Exp. Environ. Eng. Sci. 15 (3), 215–224.

Elimelech, M., Gregory, J., Jia, X., Williams, R.A., 1995. Particle Deposition and Aggregation: Measurement, Modeling and Simulation. Butterworth-Heinemann Ltd., Oxford.

Ferretti, R., Stoll, S., Zhang, J.W., Buffle, J., 2003. Flocculation of hematite particles by a comparatively large rigid polysaccharide: schizophyllan. J. Colloid Interface Sci. 266 (2), 328–338.

Francois, R.J., 1987. Strength of aluminium hydroxide flocs. Water Res. 21, 1023–1030.

Francois, R.J., 1988. Growth kinetics of hydroxide flocs. J. Am. Water Works Assoc. 80, 92–96.

Furrer, G., Ludwig, C., Schindler, P.W., 1992. On the chemistry of the Keggin Al_{13} polymer. 1. Acid–base properties. J. Colloid Interface Sci. 149, 56–67.

Gregory, J., 1973. Rates of flocculation of latex particles by cationic polymers. J. Colloid Interface Sci. 42, 448–456.

Jarvis, P., Jefferson, B., Gregory, J., Parsons, S.A., 2005. A review of floc strength and breakage. Water Res. 39, 3121–3137.

Jiang, Q., Logan, B.E., 1996. Fractal dimensions of aggregates from shear devices. J. Am. Water Works Assoc. 88 (2), 100–113.

Katz, A., Bentur, A., Kovler, K., 2007. A novel system for in-situ observations of early hydration reactions in wet conditions in conventional SEM. Cement Concrete Res. 37, 32–37.

Letterman, R.D., Quon, J.K., Gemmel, R.S., 1973. Influences of rapid mix parameters on flocculation. J. Am. Water Works Assoc. 65, 716–725.

Li, J., Fitz-Gerald, J.M., Oberhauser, J.P., 2007. Novel wet SEM imaging of organically modified montmorillonite clay dispersions. Appl. Phys. A – Mater. 87, 97–102.

Licskó, I., 1997. Realistic coagulation mechanisms in the use of aluminium and iron (III) salts. Water Sci. Technol. 36 (4), 103–110.

Lin, M.Y., Lindsay, H.M., Weitz, D.A., Ball, R.C., Klein, R., Meakin, P., 1989. Universality in colloid aggregation. Nature 339, 360–362.

Lin, J.L., Huang, C.P., Pan, J.R., Wang, D.S., 2008. Effect of Al(III) speciation on coagulation of highly turbid water. Chemosphere 72, 189–196.

Lin, J.-L., Chin, C.-J., Huang, C., Pan, J.R., Wang, D., 2008. Coagulation behavior of Al13 aggregates. Water Research 42, 4281–4290.

Liu, G.G., Qu, J.H., Tang, H.G., 1999. The electrochemical production of highly effective polyaluminum chloride. Water Res. 33 (3), 807–813.

Matsui, Y., Yuasa, A., Furuya, Y., Kamei, T., 1998. Dynamic analysis of coagulation with alum and PACl. J. Am. Water Works Assoc. 90 (10), 96–106.

McCurdy, K., Carlson, K., Gregory, D., 2004. Floc morphology and cyclic shearing recovery: comparison of alum and polyaluminum chloride coagulants. Water Res. 38, 486–494.

Oles, V., 1992. Shear-induced aggregation and breakup of polystyrene late particles. J. Colloid Interface Sci. 154, 351–358.

Parker, D.R., Bertsch, P.M., 1992. Identification and quantification of the Al_{13} tridecameric polycation using ferron. Environ. Sci. Technol. 26, 908–914.

Phillips, B.L., Casey, W.H., Karlsson, M., 2000. Bonding and reactivity at oxide mineral surfaces from model aqueous complexes. Nature 404, 379–382.

Shi, B.Y., Li, G.H., Wang, D.S., Tang, H.X., 2007. Separation of Al_{13} from polyaluminum chloride by sulfate precipitation and nitrate metathesis. Sep. Purif. Technol. 54, 88–95.

Thomas, D.N., Judd, S.J., Fawcett, N., 1999. Flocculation modeling: a review. Water Res. 33, 1579–1592.

Torres, F.E., Russel, W.B., Schowalter, W.R., 1991. Simulations of coagulation in viscous flows. J. Colloid Interface Sci. 145, 51–73.

Van Benschoten, J.E., Edzwald, J.K., 1990. Chemical aspects of coagulation using aluminum slats-2. Coagulation of fulvic acid using alum and polyaluminum chloride. Water Res. 24 (12), 1519–1526.

Waite, T.D., Cleaver, J.K., Beattie, J.K., 2001. Aggregation kinetics and fractal structure of γ-alumina assemblages. J. Colloid Interface Sci. 241, 333–339.

Wang, D.S., Tang, H.X., Gregory, J., 2002. Relative importance of charge neutralization and precipitation on coagulation of kaolin with PACl: effect of sulfate ion. Environ. Sci. Technol. 36, 1815–1820.

Wang, D.S., Sun, W., Xu, Y., Tang, H.X., Gregory, J., 2004. Speciation stability of inorganic polymer flocculant–PACl. Colloid Surf. A 243, 1–10.

Wang, W.Z., Hsu, P.H., 1994. The nature of polynuclear OH–Al complexes in laboratory-hydrolyzed and commercial hydroxyaluminum solutions. Clays Clay Miner. 42, 356–368.

Wood, T.E., Siedle, A.R., Hill, J.R., Skarjune, R.P., Goodbrake, C.J., 1990. Hydrolysis of aluminium. Are all gels created equal? In: Better Ceramic through Chemistry IV, Material Res. Sco. Symp. Proc. Pittsburgh, vol. 180, pp. 97–116.

Wu, R.M., Lee, D.J., Waite, T.D., Guan, J., 2002. Multilevel structure of sludge flocs. J. Colloid Interface Sci. 252, 383–392.

Ye, C.Q., Wang, D.S., Shi, B.Y., Yu, J.F., Qu, J.H., Edwards, M., Tang, H.X., 2007. Alkalinity effect of coagulation with polyaluminum chlorides: role of electrostatic patch. Colloid Surf. A 294, 163–173.

Yu, J.F., Wang, D.S., Ge, X.P., Yan, M.Q., Yang, M., 2006. Flocculation of kaolin particles by two typical polyelectrolytes: a comparative study on the kinetic and flocs structures. Colloid Surf. A 290, 288–294.

Zbik, M., Horn, R.G., 2003. Hydrophobic attraction may contribute to aqueous flocculation of clays. Colloid Surf. A 222, 323–328.

Zhou, Y., Franks, G.V., 2006. Flocculation mechanism induced by cationic polymers investigated by light scattering. Langmuir 22, 6775–6786.